Design and Vehicle Implementation of Preview Active Suspension Controllers

Christoph Göhrle, Andreas Schindler, Andreas Wagner, and Oliver Sawodny

***Abstract*— Active suspensions influencing the vertical dynamics of vehicles enable the improvement of ride comfort and handling characteristics compared to vehicles with passive suspensions. If the road height profile in front of the car is measured using vehicle sensors, more efficient control strategies can be applied. In this brief, two model predictive approaches for preview active suspension controllers are proposed and compared to the well-known optimal preview control approach. The considered active suspension consists of low bandwidth actuators in series with the spring and passive dampers. Equations of a linear full-car model are derived. The first model predictive controller optimizes the actuator displacements on a nonequidistant grid over the preview horizon. The second controller optimizes trajectories for heave, pitch, and roll of the vehicle body over the preview horizon using a quadratic program. Therefore, a model inversion is presented. The trajectories are formulated as a summation of nonequidistant B-spline basis functions and constraints on the input are incorporated in trajectory generation via the inverse vehicle model. Simulation results are presented and vehicle implementation using recorded road height data is conducted.**

***Index Terms*— Active vehicle suspension, model predictive control (MPC), road preview, trajectory generation, vehicle dynamics.**

I. Introduction

An IMPORTANT goal in vehicle development is constantly improving ride comfort and handling characteristics. Active suspensions that influence the vertical dynamics of vehicles can improve ride comfort and handling over vehicles with passive suspensions. Several advanced driver assistance systems in modern vehicles are using sensors to detect the surroundings of the car. For example, a lane departure warning system detects the lane in front of the car. There are systems that detect pedestrians and other vehicles and brake automatically to avoid or reduce the impact of an accident. Additionally systems that recognize traffic signs and inform the driver are available on the market. Possible sensors for these functions are a mono or stereo camera, a laser sensor, or a photonic mixing device. These sensors can also be used to measure the road height profile in front of the car with a certain accuracy, as shown in Fig. 1. The capability of different sensors to accurately measure the road height in front of the vehicle is currently evaluated in the automotive industry.

Manuscript received June 19, 2012; revised May 10, 2013; accepted June 8, 2013. Manuscript received in final form July 2, 2013. Date of publication July 26, 2013; date of current version April 17, 2014. This work was supported by Audi AG. Recommended by Associate Editor J. Lu.

C. Göhrle and O. Sawodny are with the Institute for System Dynamics, University of Stuttgart, Stuttgart 70569, Germany (e-mail: christoph.goehrle@isys.uni-stuttgart.de; sawodny@isys.uni-stuttgart.de).

A. Schindler and A. Wagner are with Audi AG, Ingolstadt 85045, Germany (e-mail: andreas.schindler@audi.de; andreas5.wagner@audi.de).

Color versions of one or more of the figures in this paper are available online at http://ieeexplore.ieee.org.

Digital Object Identifier 10.1109/TCST.2013.2272342

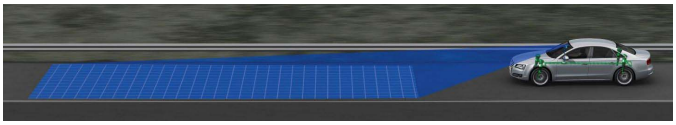

Fig. 1. Vehicle with active suspension and preview information.

With this additional information, more efficient controllers for semiactive and active suspensions are feasible. Current vehicles can only react to road disturbances, with preview it is possible to proactively control the actuators considering actuator dynamics and constraints. In this brief, the road height profile in front of the car is assumed to be known and possible controllers will be discussed. The main goal is to compensate the road unevenness with actuators between wheel and vehicle body, allowing the vehicle body to remain as smooth as possible to improve ride comfort. Improved ride comfort can be measured by a reduction of vehicle body acceleration. Active suspension controllers also need to maintain handling characteristics and ride safety. This can be quantified by good road holding and hence low dynamic wheel load fluctuation.

A preview active suspension controller was first discussed in [1] using a transfer function to calculate the actuator excursion from the road height profile. [2] applies a multi-criteria control design based on a half car-model with off-line optimized transfer functions for the feedforward part and gains for the feedback part. Many studies [3]–[9] are using a quarter-car model of the plant and the Hamiltonian approach of optimal control. This results in a linear-quadratic regulator as state feedback and a preview feedforward term calculated from the oncoming road height profile. References [10] and [11] are using a half-car model and the optimal preview control approach, [12] also employs the optimal preview control approach and furthermore applies a road-sensing system in a vehicle. Reference [13] uses a H_∞ controller and verifies the results with a quarter vehicle suspension system and [14] uses H_∞ control for active suspensions without preview. Reference [15] applies a preview active suspension system in a vehicle with laser sensors to measure the road height profile. A survey over optimal control for vehicle suspensions is given in [16].

The aforementioned controllers cannot explicitly incorporate constraints on the control variable. Because actuator displacement and actuator displacement rate are limited, model predictive control seems to be the appropriate controller design scheme. Reference [17] and [18] are applying model predictive control (MPC) for active suspensions with preview information based on a quarter-car model, [19] uses a half-car model and MPC. In this brief, two model predictive approaches based on a reduced full-car model are proposed and compared to the optimal preview control approach.

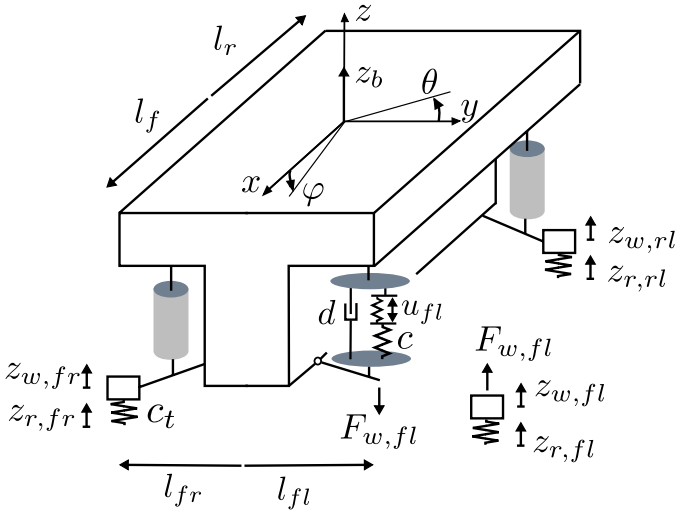

Fig. 2. Full-car model.

II. Vehicle Model

Equations of motion for a seven degree of freedom full-car model of vertical dynamics, shown in Fig. 2, are derived as follows. There are the heave (z_b), pitch (φ), and roll (θ) degree of freedom of the vehicle body. The vertical displacements of the wheels are denoted $z_{w,ii}$, where throughout this brief $ii \in \{fl, fr, rl, rr\}$ stands for front/rear left/right. Furthermore, vectors denote the variable on each wheel written in a column, e.g., $\underline{z}_w = \left(z_{w,fl}\ z_{w,fr}\ z_{w,rl}\ z_{w,rr}\right)^T$. The tire is modeled as a spring and $z_{r,ii}$ denotes the vertical road disturbance under every tire. The vehicle suspension considered in this brief consists of passive dampers with damper force $F_{d,ii}$ and four actuators in series with the primary spring with spring force $F_{c,ii}$. The actuator is described by its displacement u_{ii} and energy-saving low bandwidth actuators with a frequency up to 5 Hz are considered. To support the vehicle body steady-state without losing energy, a spring parallel to the actuator is necessary as depicted but does not influence the equations of motion.

A. Equations of Motion for the Vehicle Body

Conservation of momentum for the vehicle body with the assumption of small angles of pitch and roll and decoupled vehicle body dynamics is set up

$$\underbrace{\begin{pmatrix} m_b & 0 & 0 \\ 0 & J_\varphi & 0 \\ 0 & 0 & J_\theta \end{pmatrix}}_{\Theta_b} \cdot \begin{pmatrix} \ddot{z}_b \\ \ddot{\varphi} \\ \ddot{\theta} \end{pmatrix} = -\mathbf{T}_G \cdot \underbrace{\begin{pmatrix} F_{w,fl} \\ F_{w,fr} \\ F_{w,rl} \\ F_{w,rr} \end{pmatrix}}_{\underline{F}_w}$$

$$\mathbf{T}_G = \begin{pmatrix} 1 & 1 & 1 & 1 \\ -l_f & -l_f & l_r & l_r \\ l_{fl} & -l_{fr} & l_{rl} & -l_{rr} \end{pmatrix}. \quad (1)$$

The product of inertia $J_{\varphi\theta}$ of a typical passenger vehicle accounts for less than 1 % of the moment of inertia J_θ. Hence, it is neglected and there are only diagonal elements in the matrix Θ_b. The constant m_b denotes the mass of the vehicle body. Wheel base is considered by l_f and l_r, track width by l_{ii}. In contrast to [12] and [16], the proposed full-car model incorporates more realistic mechanics of the suspension by introducing the ratio i_d between wheel and damper and the ratio i_c between wheel and spring with

$$F_{w,ii} = i_{d,ii} \cdot F_{d,ii} + i_{c,ii} \cdot F_{c,ii}. \quad (2)$$

Both ratios can be determined through vehicle suspension deflection tests. The spring and damper forces are defined by

$$\begin{aligned} \underline{F}_c &= \mathbf{K}_c \cdot \left(\underline{z}_{\text{rel},c} - \underline{u}\right) \\ \underline{F}_d &= \mathbf{K}_d \cdot \underline{\dot{z}}_{\text{rel},d}. \end{aligned} \quad (3)$$

The matrices $\mathbf{K}_c$ and $\mathbf{K}_d$ comprise the spring and damper constants in the diagonal elements, and these can be different for the front and the rear axles. The vector $\underline{z}_{\text{rel},c}$ defines the relative displacement of the spring. The vector $\underline{\dot{z}}_{\text{rel},d}$ denotes the relative velocity of the damper. This relative displacement and the relative velocity can be obtained as follows:

$$\begin{aligned} \underline{z}_{\text{rel},c} &= \mathbf{T}_c^T \begin{pmatrix} z_b \\ \varphi \\ \theta \end{pmatrix} - \mathbf{H}_c \cdot \underline{z}_w \\ \underline{\dot{z}}_{\text{rel},d} &= \mathbf{T}_d^T \begin{pmatrix} \dot{z}_b \\ \dot{\varphi} \\ \dot{\theta} \end{pmatrix} - \mathbf{H}_d \cdot \underline{\dot{z}}_w \end{aligned} \quad (4)$$

with $\mathbf{T}_d = \mathbf{T}_G \cdot \mathbf{H}_d$ and $\mathbf{T}_c = \mathbf{T}_G \cdot \mathbf{H}_c$. The matrices $\mathbf{H}_c$ and $\mathbf{H}_d$ comprise the ratios of (2) in the diagonal elements. Replacing $F_{w,ii}$ in (1) in consideration of (2) and the definition for the spring and damper forces (3) leads to the following equations of motion for the vehicle body:

$$\begin{aligned} \Theta_b \begin{pmatrix} \ddot{z}_b \\ \ddot{\varphi} \\ \ddot{\theta} \end{pmatrix} + \mathbf{T}_d \mathbf{K}_d \mathbf{T}_d^T \begin{pmatrix} \dot{z}_b \\ \dot{\varphi} \\ \dot{\theta} \end{pmatrix} + \mathbf{T}_c \mathbf{K}_c \mathbf{T}_c^T \begin{pmatrix} z_b \\ \varphi \\ \theta \end{pmatrix} \\ = \mathbf{T}_d \mathbf{K}_d \mathbf{H}_d \underline{\dot{z}}_w + \mathbf{T}_c \mathbf{K}_c \mathbf{H}_c \underline{z}_w + \mathbf{T}_c \mathbf{K}_c \underline{u}. \end{aligned} \quad (5)$$

B. Equations of Motion for the Wheels

To derive the equations of motion of the wheels, conservation of momentum for the wheel masses is set up

$$\Theta_w \underline{\ddot{z}}_w = -\mathbf{K}_{c,t} \left(\underline{z}_w - \underline{z}_r\right) + \underline{F}_w \quad (6)$$

where Θ_w consists of the wheel masses and $\mathbf{K}_{c,t}$ of the tire stiffness in the diagonal elements. Eliminating the internal forces $\underline{F}_w$ in (6) leads to

$$\begin{aligned} \Theta_w \underline{\ddot{z}}_w + \mathbf{H}_d \mathbf{K}_d \mathbf{H}_d \underline{\dot{z}}_w + \left(\mathbf{H}_c \mathbf{K}_c \mathbf{H}_c + \mathbf{K}_{c,t}\right) \underline{z}_w \\ = \mathbf{H}_d \mathbf{K}_d \mathbf{T}_d^T \begin{pmatrix} \dot{z}_b \\ \dot{\varphi} \\ \dot{\theta} \end{pmatrix} + \mathbf{H}_c \mathbf{K}_c \mathbf{T}_c^T \begin{pmatrix} z_b \\ \varphi \\ \theta \end{pmatrix} - \mathbf{H}_c \mathbf{K}_c \underline{u} + \mathbf{K}_{c,t} \underline{z}_r. \end{aligned} \quad (7)$$

The equations of motion of the vehicle body (5) and the equations of motion of the wheels (7) describe a linear state–space model with the fourteen states $\underline{x}_{7dof} = \left(z_b, \varphi, \theta, \underline{z}_w, \dot{z}_b, \dot{\varphi}, \dot{\theta}, \underline{\dot{z}}_w\right)^T$, the control variable $\underline{u}$, and the measured disturbance vector $\underline{z}_r$. Actuator dynamics can be considered in the model. Assuming a first-order lag for the actuators, the state–space formulation is augmented by one state for every actuator, shown in [20].

C. Model Reduction

Actuators with a bandwidth up to 5 Hz are considered, which is below the eigenfrequency of the wheels of 12 Hz. Using the derived full-car model, a suspension controller calculates high-frequency control signals to influence wheel dynamics, which cannot be realized by the actuator. Hence, wheel dynamics are neglected in the model. This was also proposed by [21], but is not a common approach in the literature. Using the reduced model without modeled wheel dynamics, the controller calculates control signals in a feasible frequency range. Furthermore, vertical displacement of the wheels and vertical velocity of the wheels are no states of the reduced model and hence do not have to be observed for controller implementation.

To derive the reduced model, tire deflections $\underline{z}_{\text{def}}$ with $\underline{z}_w = \underline{z}_{\text{def}} + \underline{z}_r$ are introduced. In (5) and in (7) $\underline{z}_w$ is replaced by this equation. In the resulting equation of motion of the wheels, the dynamic parts are eliminated and a steady-state tire deflection is calculated. This steady-state tire deflection is inserted in the resulting equation of motion of the vehicle body, which leads to a reduced model with the three degrees of freedom of heave, pitch, and roll

$$\begin{aligned}
\dot{\underline{x}}(t) &= \begin{pmatrix} 0_{3\times 3} & I_3 \\ -\Theta_b^{-1}\left(\mathbf{T}_c\mathbf{K}_c\mathbf{T}_c^T - \mathbf{T}^*\mathbf{A}^*\right) & -\Theta_b^{-1}\mathbf{T}_d\mathbf{K}_d\mathbf{T}_d^T \end{pmatrix}\underline{x}(t) \\
&\quad + \begin{pmatrix} 0_{3\times 4} \\ \Theta_b^{-1}\left(\mathbf{T}_c\mathbf{K}_c - \mathbf{T}^*\mathbf{B}^*\right) \end{pmatrix}\underline{u}(t) \\
&\quad + \begin{pmatrix} 0_{3\times 4} & 0_{3\times 4} \\ \Theta_b^{-1}\mathbf{T}^*{\mathbf{H}^*}^{-1}\mathbf{K}_{c,t} & \Theta_b^{-1}\mathbf{T}^*\mathbf{T}_d\mathbf{K}_d\mathbf{H}_d \end{pmatrix}\underline{w}(t) \\
\underline{x} &= \left(z_b\ \varphi\ \theta\ \dot{z}_b\ \dot{\varphi}\ \dot{\theta}\right)^T \\
\underline{w} &= \left(\underline{z}_r\ \dot{\underline{z}}_r\right)^T \\
\mathbf{A}^* &= {\mathbf{H}^*}^{-1}\mathbf{H}_c\mathbf{K}_c\mathbf{T}_c^T \\
\mathbf{B}^* &= {\mathbf{H}^*}^{-1}\mathbf{H}_c\mathbf{K}_c \\
\mathbf{T}^* &= \mathbf{T}_c\mathbf{K}_c\mathbf{H}_c \\
\mathbf{H}^* &= \mathbf{H}_c\mathbf{K}_c\mathbf{H}_c + \mathbf{K}_{c,t}.
\end{aligned} \tag{8}$$

This formulation has both the road height and the first derivative of the road height as inputs.

III. Model Predictive Controller

In this section, a model predictive controller which optimizes the actuator displacements $\underline{u}$ on a nonequidistant grid over the preview horizon is proposed. Constraints on the input $\underline{u}$ are incorporated.

A. Output Prediction

A zero-order hold discretization of the reduced vehicle model (8) is conducted. Control variables and road height profile are assumed to be constant between defined steps, where these steps are multiples of the sampling time. The main goal of a preview active suspension control is to improve ride comfort. Hence, the output $\underline{y} = \left(\ddot{z}_b, \ddot{\varphi}, \ddot{\theta}\right)^T$ is predicted for the time steps k_1 to k_n

$$\begin{aligned}
\hat{\underline{y}} &= \hat{\Phi}\underline{x}[k] + \hat{\Gamma}_{u,k}\underline{u}[k] + \hat{\Gamma}_u\hat{\underline{u}} + \hat{\Gamma}_w\hat{\underline{w}} \\
\hat{\underline{y}} &= \begin{pmatrix} \underline{y}[k+k_1] \\ \vdots \\ \underline{y}[k+k_n] \end{pmatrix}\hat{\underline{u}} = \begin{pmatrix} \underline{u}[k+k_1] \\ \vdots \\ \underline{u}[k+k_n] \end{pmatrix}\hat{\underline{w}} = \begin{pmatrix} \underline{w}[k] \\ \vdots \\ \underline{w}[k+k_n] \end{pmatrix}.
\end{aligned} \tag{9}$$

The matrices $\hat{\Phi}$, $\hat{\Gamma}_{u,k}$, $\hat{\Gamma}_u$, and $\hat{\Gamma}_w$ can be calculated from the state–space matrices from (8).

B. Quadratic Program

The following cost function over the prediction horizon is minimized, the end state is especially weighted:

$$\min_{\hat{\underline{u}}}\left(\hat{\underline{y}}^T\mathbf{Q}\hat{\underline{y}} + \hat{\underline{u}}^T\mathbf{R}\hat{\underline{u}}\right). \tag{10}$$

Inserting the output over the prediction horizon (9) in the cost function (10) and omitting the terms not dependent on the optimization variable leads to the following expression, which is similar to the approaches in [17]–[19]:

$$\begin{aligned}
&\min_{\hat{\underline{u}}}\ \frac{1}{2}\hat{\underline{u}}^T\left(\hat{\Gamma}_u^T\mathbf{Q}\hat{\Gamma}_u + \mathbf{R}\right)\hat{\underline{u}} \\
&+ \left(\underline{x}[k]^T\hat{\Phi}^T\mathbf{Q}\hat{\Gamma}_u + \underline{u}[k]^T\hat{\Gamma}_{u,k}^T\mathbf{Q}\hat{\Gamma}_u + \hat{\underline{w}}^T\hat{\Gamma}_w^T\mathbf{Q}\hat{\Gamma}_u\right)\hat{\underline{u}}.
\end{aligned} \tag{11}$$

Actuator displacement and actuator displacement rate are mechanically limited and these constraints are incorporated. This is equivalent to a quadratic program

$$\begin{aligned}
\min_{\hat{\underline{u}}}\quad & \tfrac{1}{2}\hat{\underline{u}}^T\mathbf{H}\hat{\underline{u}} + \underline{g}^T\hat{\underline{u}} \\
\text{s.t.}\quad & \hat{\underline{u}}_{\min} \le \hat{\underline{u}} \le \hat{\underline{u}}_{\max} \\
& \Delta\hat{\underline{u}}_{\min} \le \Delta\hat{\underline{u}} \le \Delta\hat{\underline{u}}_{\max}.
\end{aligned} \tag{12}$$

Incorporating constraints on suspension deflection to not hit the bump stoppers result in the additional constraints $\underline{l} \le \mathbf{M}\hat{\underline{u}} \le \underline{b}$.

IV. Model Inversion

In the literature, the authors use quarter-car [9], half-car [10] and in some cases full-car models [12] with the actuator and the road unevenness as input and the vehicle behavior as output. In this section, the authors propose to invert the vehicle model, which will be necessary for the model predictive trajectory generation presented in Section V. In contrast to the seven degree of freedom full-car model, derived in Section II, the reduced state–space model (8) is controllable and the three states heave, pitch, and roll are flat outputs (for definition, see [22]) of the system with the special feature that the system with one vehicle body mass and four actuators is overdetermined. There are four inputs for the three outputs $\underline{z} = (z_b, \varphi, \theta)^T$ and hence one additional degree of freedom can be chosen. It is proposed to eliminate warping in the vehicle body. Hence, on a flat road, all four actuators are supporting the same load. It is defined that the sum of the steady-state forces of the actuator's front left and rear right equals to the sum of the forces of the actuator's front right and rear left

$$\left(-1\ 1\ 1\ -1\right)\left(\mathbf{T}_c^T\underline{z} - \mathbf{H}_c\underline{z}_r - \underline{u}\right) = 0. \tag{13}$$

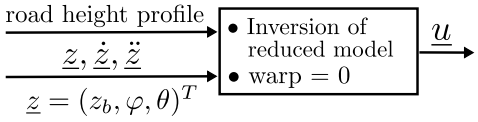

Fig. 3. Inverse vehicle model.

Equations (8) and (13) lead to a model inversion of the reduced full-car model (8), which is depicted in Fig. 3

$$\underline{u} = \mathbf{K}_0\underline{z} + \mathbf{K}_1\dot{\underline{z}} + \mathbf{K}_2\ddot{\underline{z}} + \mathbf{K}_3\underline{w}. \tag{14}$$

V. Model Predictive Trajectory Generation

In Section III, a model predictive controller, optimizing the actuator displacements over a nonequidistant grid, was presented. In this section, a model predictive controller optimizing the trajectories for heave, pitch, and roll is proposed, the same nonequidistant grid and the same constraints on the input (12) as for the first controller are incorporated. The receding horizon real-time trajectory generation is set up to minimize heave, pitch, and roll acceleration. The framework nonlinear trajectory generation (NTG) for nonlinear real-time trajectory generation based on B-spline parameterization of the output is presented in [23] and [24]. The following presented trajectory optimization differs, because preview information can be incorporated and the initial values of the trajectories are computed from the initial vehicle state. In the NTG framework, the initial values are optimization variables, which can be constrained. It will be shown that the presented approach leads to a quadratic program. The main advantage of the model predictive trajectory generation compared to the model predictive control, presented in Section III, are the reduced number of optimization variables, as heave, pitch, and roll instead of four actuator signals are optimized. Furthermore, if the optimization fails because of infeasibility or computational effort, the optimal trajectories can be replaced by zeros to calculate the actuator signal using the inverse model (14). Setting the trajectories to zero does not incorporate constraints and initial vehicle state, but still results in good performance.

A. Nonuniform B-Spline

As in [23], the output $\underline{z}$ is parameterized in terms of B-spline curves, the concept of B-splines is discussed in [25]. Cubic B-splines are chosen because this is the lowest possible degree to be $\mathcal{C}^2$ continuous, which is necessary for the inverse model (14): $z_1(t) = \sum_{i=0}^{m-5} P_i b_i(t) \quad t \in [t_3, t_{m-4}]$. The knot vector with m knots $t_0 \le t_1 \le \cdots \le t_{m-1}$ defines the basis functions $b_i(t)$ of a B-spline, P_i denote the control points weighting the basis functions. The derivative of the basis functions can be calculated in advance and hence the trajectory and the first and second-derivative of the trajectory can be expressed as a function of a set of control points. The knot vector is chosen once and the piecewise-defined cubic B-spline can also be written in matrix notation

$$z_{1,i}(t) = \begin{pmatrix} A_i(t) & B_i(t) & C_i(t) & D_i(t) \end{pmatrix} \begin{pmatrix} P_{i-1} \\ P_i \\ P_{i+1} \\ P_{i+2} \end{pmatrix}$$
$$t \in \left[t_{i+2}, t_{i+3}\right] \qquad i \in \{1, 2, \ldots, m-7\}. \tag{15}$$

The outputs z_2 and z_3 are defined equivalently.

B. Cost Function

The optimization is set up to minimize the second derivatives of the three trajectories for heave, pitch, and roll over the preview horizon. The cost function is defined to be evaluated at the knots of the B-spline basis functions at points $\underline{T}$ with $\underline{T} = (t_4, \ldots, t_{m-4})$. The knot t_3 is set to zero and indicates the initial time. The knot vector is chosen to be the same for the three trajectories. $\underline{P}_1 = \left(P_{1,h}, P_{1,p}, P_{1,r}\right)^T$ denote the second control point for the heave, pitch, and roll trajectory. The second derivative of the three trajectories at points $\underline{T}$ is calculated

$$\ddot{\underline{z}} = \underbrace{\begin{pmatrix} \ddot{\mathbf{A}}_2 & \ddot{\mathbf{B}}_2 & \ddot{\mathbf{C}}_2 & \ddot{\mathbf{D}}_2 & & \\ & \ddot{\mathbf{A}}_3 & \ddot{\mathbf{B}}_3 & \cdots & & \\ & & & & \ddots & \end{pmatrix}}_{\left(\int_2^* \mathcal{S}_2\right)} \begin{pmatrix} \underline{P}_1 \\ \underline{P}_2 \\ \\ \vdots \\ \underline{P}_{m-5} \end{pmatrix}$$
$$\ddot{\underline{\hat{z}}} = \left(\ddot{\underline{z}}(t_4) \ \ldots \ \ddot{\underline{z}}(t_{m-4})\right)^T. \tag{16}$$

$\ddot{\mathbf{A}}_i$ comprises $\ddot{A}_i(\underline{T}(i-1))$ in the three diagonal elements, $\ddot{\mathbf{B}}_i$, $\ddot{\mathbf{C}}_i$ and $\ddot{\mathbf{D}}_i$ equivalently. The vector $\hat{\underline{p}}$ consists of optimization variables, with $\hat{\underline{p}} = \left(\underline{P}_3, \ldots, \underline{P}_{m-5}\right)^T$. The first three control points of the trajectories $\underline{P}_0$, $\underline{P}_1$, and $\underline{P}_2$ are determined by the initial vehicle state, which is to be observed online

$$\begin{pmatrix} \underline{P}_0 \\ \underline{P}_1 \\ \underline{P}_2 \end{pmatrix} = \begin{pmatrix} \mathbf{A}_1 & \mathbf{B}_1 & \mathbf{C}_1 \\ \dot{\mathbf{A}}_1 & \dot{\mathbf{B}}_1 & \dot{\mathbf{C}}_1 \\ \ddot{\mathbf{A}}_1 & \ddot{\mathbf{B}}_1 & \ddot{\mathbf{C}}_1 \end{pmatrix}^{-1} \begin{pmatrix} \underline{z}_0 \\ \dot{\underline{z}}_0 \\ \ddot{\underline{z}}_0 \end{pmatrix}. \tag{17}$$

$\mathbf{D}_1$ is zero if knot t_3 is chosen to zero. $\mathbf{A}_1$ comprises $A_1(0)$ in the three diagonal elements, the other matrices are defined equivalently. A quadratic cost function to minimize the second derivative of the three trajectories at points $\underline{T}$ is formulated

$$\min_{\hat{\underline{p}}} \ \ddot{\underline{\hat{z}}}^T \mathbf{Q}_p \ddot{\underline{\hat{z}}} =$$
$$\min_{\hat{\underline{p}}} \ \left(\underline{\int}_2 + \mathcal{S}_2\hat{\underline{p}}\right)^T \mathbf{Q}_p \left(\underline{\int}_2 + \underline{\mathcal{S}}_2\hat{\underline{p}}\right) =$$
$$\min_{\hat{\underline{p}}} \ \hat{\underline{p}}^T \mathcal{S}_2^T \mathbf{Q}_p \mathcal{S}_2 \hat{\underline{p}} + 2\hat{\underline{p}}^T \mathcal{S}_2^T \mathbf{Q}_p \underline{\int}_2 \tag{18}$$

$$\underline{\int}_2 = \int_2^* \cdot \begin{pmatrix} \underline{P}_1 \\ \underline{P}_2 \end{pmatrix}. \tag{19}$$

Weighting of the control variable is possible but omitted in (18) to obtain a quadratic program with constant Hessian Matrix. The control variable $\underline{u}$ is calculated via the inverse model and hence dependent of the road height profile. Not weighting the control variable can be compensated for by an appropriate choice of $\mathbf{Q}$ and weighting of the end control points.

C. Quadratic Program With Constraints

The control variables $\underline{\hat{u}}$ at the knots of the B-spline basis functions at points $\underline{T}$ are expressed as a function of the optimization variables $\underline{\hat{p}}$ using the inverse model (14)

$$\underline{\hat{u}} = (\mathcal{K}_0\mathcal{S}_0 + \mathcal{K}_1\mathcal{S}_1 + \mathcal{K}_2\mathcal{S}_2)\,\underline{\hat{p}} + \mathcal{K}_0\underline{\int}_0 + \mathcal{K}_1\underline{\int}_1 + \mathcal{K}_2\underline{\int}_2 + \mathcal{K}_3\underline{\hat{w}}. \tag{20}$$

The constant matrix $\mathcal{S}_0$ and the constant vector $\underline{\int}_0$ for the trajectory and $\mathcal{S}_1$, $\underline{\int}_1$ for the first derivative of the trajectory are defined equivalently to $\mathcal{S}_2$, $\underline{\int}_2$ from (16) and (19). $\mathcal{K}_0$ denotes a matrix with $\mathbf{K}_0$ from (14) on the diagonal elements. The same applies for $\mathcal{K}_1$, $\mathcal{K}_2$, and $\mathcal{K}_3$.

The same constraints as for the first controller (12) are incorporated. Using (20), the input constraints on $\underline{\hat{u}}$ are mapped to constraints on the control points $\underline{\hat{p}}$. This results in an optimization (18) with constraints of the following form:

$$\begin{aligned} \min_{\underline{\hat{p}}} \quad & \tfrac{1}{2}\underline{\hat{p}}^T\mathbf{H}_p\underline{\hat{p}} + \underline{g}_p^T\underline{\hat{p}} \\ \text{s.t.} \quad & \underline{l}_p \le \mathbf{M}_p\underline{\hat{p}} \le \underline{u}_p. \end{aligned} \tag{21}$$

As with the first controller, the Hessian Matrix $\mathbf{H}_p$ is constant. Without constraints, the optimization minimizes the second derivative of the trajectories for the given initial vehicle state. System dynamics and the road height profile over the preview horizon are considered in the constraints, which ensure that actuator displacement and actuator displacement rate do not exceed the mechanically given limits. After optimizing the trajectories, the actuator signals have to be obtained via the inverse model (14).

VI. Simulation Results

A. Simulation Design

Simulation results of the presented model predictive controller and the presented model predictive trajectory generation are compared with the optimal preview control approach, presented in [9]. The optimal control approach was also set up based on the reduced vehicle model (8). Because this approach cannot incorporate constraints on the input, a saturation of actuator rate and actuator travel is added. The weighting matrices $\mathbf{Q}$ and $\mathbf{R}$ were optimized to obtain good results over the four road profiles and the same set of weighting matrices were used for the four simulations. Furthermore, results for the same vehicle with actuator travel equal to zero are depicted. This symbolizes a passive vehicle. Sampling time is set to 10 ms, preview time to 0.5 s. To solve the quadratic program, qpOASES [26] was used. The simulation model is a validated nonlinear model of vertical dynamics.

B. Simulation Results

In Fig. 4, it is exemplarily shown that the three preview controllers effect major reduction of heave acceleration by applying actuator motion inverse to the road height. The same applies to the pitch acceleration. Dynamic wheel load fluctuation is equally reduced. Fig. 5 shows the model predictive controllers lifting the vehicle body as soon as the high road

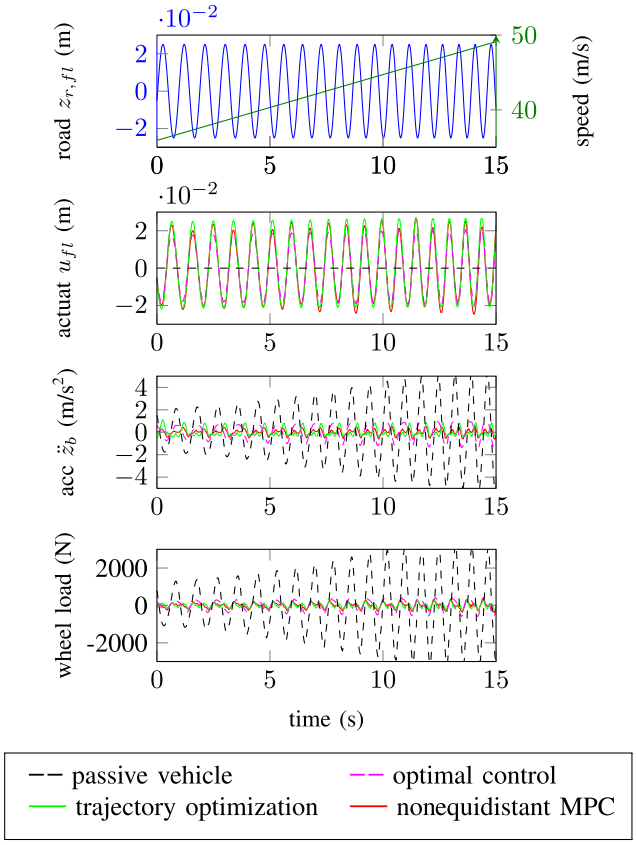

Fig. 4. Simulation: Car driving over sine wave-shaped road with increasing speed.

TABLE I
RMS Values of the Simulation Results

	Fig. 4 rms $\ddot{z}_b$	Fig. 5 rms $\ddot{z}_b$	Fig. 6 rms $\ddot{\theta}$	Fig. 7 rms $\ddot{z}_b$
passive vehicle	2.54	1.29	1.75	0.92
optimal control	0.67	1.42	0.89	0.68
trajectory optimization	0.37	0.77	0.48	0.65
non-equidistant MPC	0.25	0.77	0.50	0.64

elevation is in sight, because actuator travel is constrained in the optimization. Raising the vehicle increases actuator travel in one direction to better compensate the road elevation afterward. This results in better compensation of the obstacle as the preview optimal control approach, where the actuator travel is saturated. Fig. 6 shows the vehicle driving over a speed bump on the left side while the wheels on the right side are driving over a flat road. The two model predictive approaches minimize roll acceleration more effectively by proactive engagement of the actuators with maximum actuator speed. Proactive actuation is obtained, because constraints on the actuator displacement rate are incorporated. The second engagement of the actuator is because of the rear axle driving over the elevation. Fig. 7 shows a vehicle driving over an uneven road. It can be seen that performance is improved by the three preview controllers up to 4 Hz, because of the limitations of the given low bandwidth active suspension system. At higher frequencies, performance is equal to a system with actuator displacement equal to zero. Numerical values of the simulation results are given in Table I.

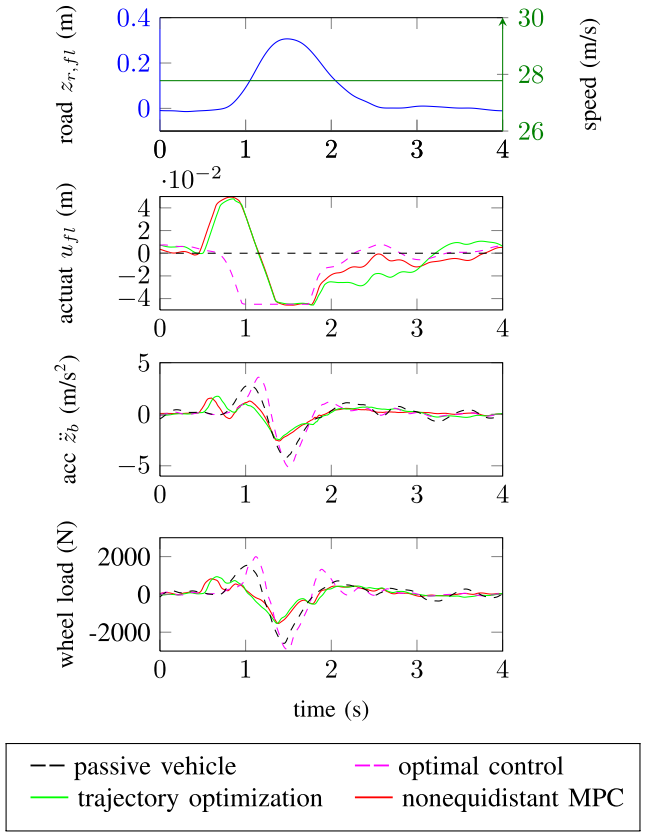

Fig. 5. Simulation: Car driving over high road elevation with constant speed.

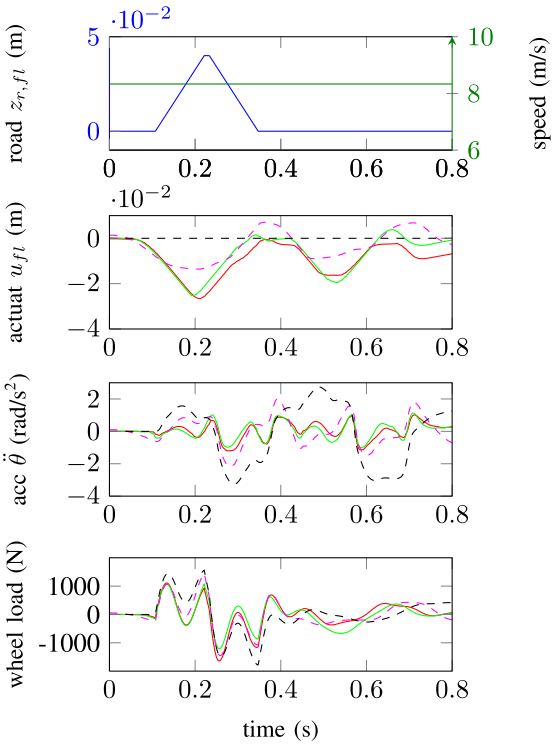

Fig. 6. Simulation: Car driving over a speed bump on the left side at constant speed.

The four simulations show that dynamic wheel load fluctuation is also reduced without having been considered in the cost function. Thus, for low bandwidth active suspension systems, improvement of ride comfort also incorporates a reduction of dynamic wheel load fluctuation.

C. Discussion of Simulation Results and Parameter Choice

A preview time of 0.5 s is defined for both MPCs and nine optimization points are distributed identically for both controllers and nonequidistantly within the given preview time. This preview time was chosen to allow the controller to lift the vehicle in front of the high road elevation in Fig. 5. For the other simulations, a preview time of 0.2 s is sufficient for the same results. The optimization was carried out on a nonequidistant grid to reduce optimization variables, as it is sufficient if the calculated control signal is less detailed in the distance.

There are two main advantages of the proposed MPCs compared to the preview optimal control approach. First, the MPCs realize proactive engagement of the actuators, because of the incorporation of actuator constraints. In Fig. 5, the vehicle is lifted in front of the high road elevation to increase the constrained actuator travel in one direction and in Fig. 6 the actuator is engaged proactively with maximum actuator speed because of the constrained actuator rate. This results in better performance than the optimal control approach. Increasing the values of $\mathbf{Q}$ with respect to $\mathbf{R}$ of the optimal control approach in Fig. 6 effects higher actuator rate at the beginning of the obstacle, which is saturated by the added rate limitation. Proactive engagement with maximum actuator speed cannot be obtained by the optimal control approach. Second, one set of weighting matrices results in the best performance over all road profiles in contrast to the optimal control approach. Increasing the values of $\mathbf{Q}$ with respect to $\mathbf{R}$ increases the performance for the optimal control approach in Fig. 4 to the same level as the MPCs. However, this set of weighting matrices results in bad performance in Fig. 7 due to permanent exceeding and saturation of the actuator rate.

Performance of the two MPCs is about the same, but the model predictive trajectory generation optimizes three trajectories, where the MPC has to optimize four actuator signals for each time step. This leads to a reduction in optimization variables and thus computing effort. Another advantage of the model predictive trajectory generation is the possible realization of a simple controller, if the optimization fails, by setting heave, pitch, and roll to zero and by calculating the control variables via the inverse model. Furthermore, system dynamics are transferred from the optimization formulation to the constraints of the trajectory optimization. Hence, the Hessian matrix of the optimization formulation remains constant if the vehicle parameters are to be adapted online. The vehicle body mass can differ through additional passengers or loaded baggage and the linearization of the damper characteristic can differ if variable dampers are considered. Quadratic programs with constant Hessian matrix can be solved more efficiently.

VII. Vehicle Implementation

Vehicle implementation using recorded road height data instead of sensors, that measure the road height profile, is

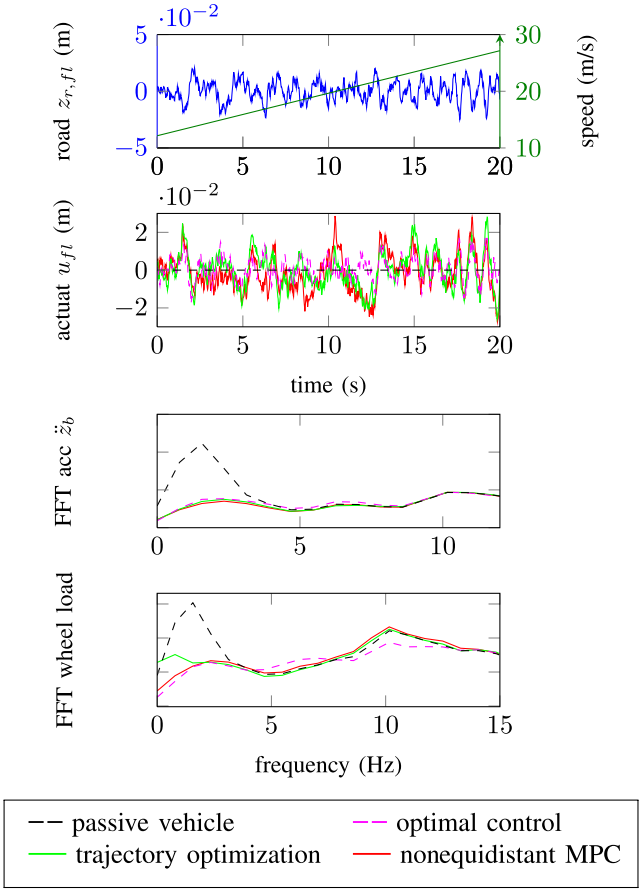

Fig. 7. Simulation: Car driving over rough road with increasing speed.

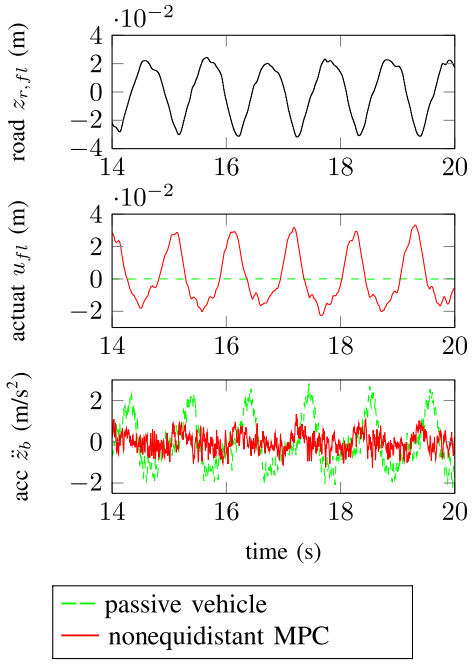

Fig. 8. Test vehicle driving over sine wave-shaped road at 120 km/h.

conducted to show the potential of a preview active suspension system. Accurate road height information for several roads was available and stored in the memory of the ECU.

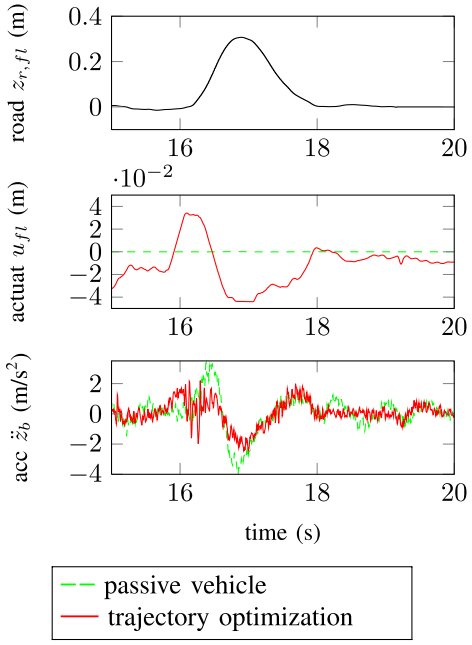

Fig. 9. Test vehicle driving over high road elevation at 100 km/h.

TABLE II
RMS VALUES OF MEASURED ACCELERATIONS

	Fig. 8 rms $\ddot{z}_b$	Fig. 9 rms $\ddot{z}_b$
passive vehicle	1.19	1.15
trajectory optimization		0.80
non-equidistant MPC	0.44	

An accurate differential global positioning system is installed in the vehicle. Thus, the road height information can be provided online for the controller and a sensor with good performance can be simulated. The presented controllers are implemented on a dSPACE AutoBox. An Audi prototype vehicle with a low bandwidth active suspension system was used. In Fig. 8, measured data of the test vehicle driving over a sine wave-shaped road, equal to the simulation in Fig. 4, at 120 km/h are presented. Fig. 9 shows the vehicle driving over a high road elevation at 100 km/h, equal to the simulation in Fig. 5. Both figures and Table II are indicating a major improvement in ride comfort equivalently to the simulation results.

VIII. CONCLUSION

In this brief, it was shown that preview active suspension control allows major improvement of ride comfort if the oncoming road height profile is measured using vehicle sensors. Therefore, simulation results over different roads for the proposed MPC, the proposed model predictive trajectory optimization, the passive vehicle, and the well-known optimal preview control approach were presented. The two model predictive approaches realize enhanced performance on two of the four presented road height profiles in comparison to the optimal preview control approach, because of an incorporation of actuator constraints. Incorporating constraints on actuator travel allow for

proactively lifting the vehicle as soon as a high road elevation is in sight to increase actuator travel and to better compensate for the obstacle. Incorporating constraints on actuator rate allow proactive actuator engagement with maximum actuator speed in front of a speed bump and hence better performance. Both presented the same performance about the effect of MPCs, but there is a reduced number of optimization variables for the model predictive trajectory generation, because heave, pitch, and roll of the vehicle body instead of four actuator displacements have to be optimized over the prediction horizon.

The controllers were implemented in a vehicle with an active suspension. The road height information was provided for the controllers using recorded road height data and an accurate differential GPS system in the vehicle. Measured data of the test vehicle driving over two different roads show a major improvement of ride comfort equivalently to the simulation results.

REFERENCES

[1] E. Bender, "Optimum linear preview control with application to vehicle suspension," *J. Basic Eng.*, vol. 90, no. 2, pp. 213–221, 1968.

[2] Q. Foag and G. Grübel, "Multi-criteria control design for preview vehicle—suspension systems," in *Proc. IFAC 10th Triennial World Congr., Munich*, 1987, pp. 1–3.

[3] M. Tomizuka, "Optimum linear preview control with application to vehicle suspension," *J. Dyn. Syst., Meas., Control*, vol. 98, no. 3, pp. 309–315, 1976.

[4] A. Thompson, B. Davis, and C. Pearce, "An optimal linear active suspension with finite road preview," Dept. Soc. Autom. Eng., Warrendale, PA, USA, Rep. SAE 800520, 1980.

[5] H. S. Roh and Y. Park, "Stochastic optimal preview control of an active vehicle suspension," *J. Sound Vibrat.*, vol. 220, no. 2, pp. 313–330, 1999.

[6] G. Prokop and R. Sharp, "Performance enhancement of limited-bandwidth active automotive suspensions by road preview," *IEE Proc. Control Theory Appl.*, vol. 142, no. 2, pp. 140–148, Mar. 1995.

[7] S. Senthil and S. Narayanan, "Optimal preview control of a two-dof vehicle model using stochastic optimal control theory," *Vehicle Syst. Dyn.*, vol. 25, no. 6, pp. 413–430, 1996.

[8] C. Pilbeam and R. S. Sharp, "Performance potential and power consumption of slow-active suspension systems with preview," *Vehicle Syst. Dyn.*, vol. 25, no. 3, pp. 169–183, 1996.

[9] A. Hac, "Optimal linear preview control of active vehicle suspension," in *Proc. 29th IEEE Conf. Decision Control*, Dec. 1990, pp. 2779–2784.

[10] J. Marzbanrad, G. Ahmadi, H. Zohoor, and Y. Hojjat, "Stochastic optimal preview control of a vehicle suspension," *J. Sound Vibrat.*, vol. 275, nos. 3–5, pp. 973–990, 2004.

[11] J. Kok, J. van Heck, R. Huisman, J. Muijderman, and F. Veldpaus, "Active and semi-active control of suspension systems for commercial vehicles based on preview," in *Proc. Amer. Control Conf.*, vol. 5. Jun. 1997, pp. 2992–2996.

[12] H.-J. Kim, H. S. Yang, and Y.-P. Park, "Improving the vehicle performance with active suspension using road-sensing algorithm," *Comput. Struct.*, vol. 80, nos. 18–19, pp. 1569–1577, 2002.

[13] A. Akbari, G. Koch, E. Pellegrini, S. Spirk, and B. Lohmann, "Multi-objective preview control of active vehicle suspensions: Experimental results," in *Proc. 2nd ICACC*, vol. 3. Mar. 2010, pp. 497–502.

[14] W. Sun, H. Gao, and O. Kaynak, "Finite frequency H_∞ control for vehicle active suspension systems," *IEEE Trans. Control Syst. Technol.*, vol. 19, no. 2, pp. 416–422, Mar. 2011.

[15] A. Schindler, "Neue Konzeption und erstmalige Realisierung eines aktiven Fahrwerks mit Preview-Strategie," Ph.D. dissertation, Karlsruher Inst. für Technol., Karlsruhe, Germany, 2009.

[16] D. Hrovat, "Survey of advanced suspension developments and related optimal control applications," *Automatica*, vol. 33, no. 10, pp. 1781–1817, 1997.

[17] B. Cho, "Active suspension controller design using MPC with preview information," *J. Mech. Sci. Technol.*, vol. 13, no. 2, pp. 168–174, 1999.

[18] R. Mehra, J. Amin, K. Hedrick, C. Osorio, and S. Gopalasamy, "Active suspension using preview information and model predictive control," in *Proc. IEEE Int. Conf. Control Appl.*, Oct. 1997, pp. 860–865.

[19] B.-K. Cho, G. Ryu, and S. J. Song, "Control strategy of an active suspension for a half car model with preview information," *Int. J. Autom. Technol.*, vol. 6, no. 1, pp. 243–249, 2005.

[20] C. Göhrle, A. Wagner, A. Schindler, and O. Sawodny, "Active suspension controller using MPC based on a full-car model with preview information," in *Proc. Amer. Control Conf., Montréal*, Jun. 2012, pp. 497–502.

[21] R. Streiter, "Entwicklung und Realisierung eines analytischen Regelkonzeptes für eine aktive Federung," Ph.D. dissertation, Dept. Electr. Eng., Technische Univ., Berlin, Berlin, Germany, 1996.

[22] A. Isidori, *Nonlinear Control Systems*. New York, NY, USA: Springer-Verlag, 1997.

[23] M. Milam, K. Mushambi, and R. Murray, "A new computational approach to real-time trajectory generation for constrained mechanical systems," in *Proc. 39th IEEE Conf. Decision Control*, vol. 1. Dec. 2000, pp. 845–851.

[24] N. Petit, M. B. Milam, and R. M. Murray, "Inversion based constrained trajectory optimization," in *Proc. 5th IFAC Symp. Nonlinear Control Syst.*, 2001, pp. 1–6.

[25] C. de Boor, *A Practical Guide to Splines*. New York, NY, USA: Springer-Verlag, 1978.

[26] H. J. Ferreau, "Model predictive control algorithms for applications with millisecond timescales," Ph.D. dissertation, Faculty Eng., Katholieke Universiteit Leuven, Leuven, Belgium, 2011.